American Mineralogist, Volume 87, pages 648–657, 2002

The high-temperature $P2_1/c$-$C2/c$ phase transition in Fe-free pyroxene ($Ca_{0.15}Mg_{1.85}Si_2O_6$): Structural and thermodynamic behavior

MARIO TRIBAUDINO,[1,*] FABRIZIO NESTOLA,[1] FERNANDO CÁMARA,[2] AND MARIA CHIARA DOMENEGHETTI[3]

[1]Dipartimento di Scienze Mineralogiche e Petrologiche, Via Valperga Caluso 35, I-10125 Torino, Italy
[2]CNR-Centro di Studio per la Cristallochimica e la Cristallografia,Via Ferrata 1, 27100 Pavia, Italy
[3]Dipartimento di Scienze della Terra, Università di Pavia, Via Ferrata 1, 27100 Pavia, Italy

ABSTRACT

A high-temperature in situ single-crystal X-ray diffraction study was performed from room T to 1150 °C on two crystals of Fe-free $P2_1/c$ clinopyroxenes of composition $Ca_{0.15}Mg_{1.85}Si_2O_6$ [cell parameters at room T: a = 9.651(2) Å, b = 8.846(2) Å, c = 5.202(1) Å, β = 108.38(2)°, V = 421.4 (2) Å^3] synthesized by isothermal annealing for 624 h at T = 1370 °C, P = 1 atm. A first order $P2_1/c$-$C2/c$ phase transition was found slightly below 1000 °C [T_c = 926(39) °C]. The transition was revealed by discontinuous changes in intensities and cell parameters. Prolonged heating at high temperature induced a non-reversible increase in the transition temperature up to more than 1150 °C, without apparent changes in the order of the phase transition. Coupling with strain due to incipient exsolution in a formerly almost defect-free sample is suggested to be responsible for increase in T_c. TEM observations of a sample from the same starting material after further annealing for 72 h at T = 1050 °C, P = 1 atm are consistent with the proposed incipient exsolution model. Annealing was found to induce the formation of a mottled texture oriented parallel to (101).

Results from structure refinement of data collected below the transition at T = 25, 500, 650, 800, and 1000 °C showed only minor changes in the chain configurations, which are highly differentiated up to 1000 °C, confirming the strong first-order character of the transition.

INTRODUCTION

Phase transitions in pyroxenes have been the subject of several investigations due to their value in determining the thermal history of the host rocks. In Ca-poor clinopyroxenes a $P2_1/c$-$C2/c$ phase transition occurs at high temperature (Smyth and Burnham 1972; Brown et al. 1972; Sueno et al. 1984) and with increasing pressure (Angel et al. 1992; Hugh-Jones et al. 1994). Structurally, this transition is driven by changes in the tetrahedral chain arrangement. In the primitive structure there are two different chains, one highly kinked (B chain) and the other more elongated (A chain), chain kinking being measured by the angle between the O3 atoms bridging the chain tetrahedra (O3-O3-O3 angle). In the $C2/c$ structure the chains become symmetrically equivalent. In the high-temperature $C2/c$ structure the two chains are elongated, whereas in the high-pressure form they are both kinked. It has been shown that the high-T (HT) and high-P (HP) $C2/c$ structures have different stability fields (Arlt et al. 2000; Arlt and Angel 2000), and that the $P2_1/c$ structure, characteristic of pigeonite clinopyroxene, is intermediate between the two varieties.

The structural changes that occur with increasing temperature and at the transition were determined by in situ high-temperature X-ray diffraction studies and the thermodynamic character of the transition was found to be first order (Brown et al. 1972; Smyth 1974; Sueno et al. 1984; Arlt and Armbruster 1997). This was demonstrated by a sudden loss, at the transition temperature, in the intensity of the $h + k$ odd reflections, which are not present in the $C2/c$ space group, (Smyth 1974) and by the coexistence of primitive and C-centered structures observed using Shimobayashi and Kitamura (1991) by high-temperature electron microscopy. However, recent TEM investigations of synthetic $Di_{40}En_{60}$-$Di_{60}En_{40}$ samples by Tribaudino (2000) have shown deviations from first-order behavior and Cámara et al. (2002) have observed a marked continuous behavior in Fe-rich samples with Ca-content up to 0.2 Ca atoms pfu. The main problem in constructing a reliable model for this transition using only data for natural clinopyroxenes is their large compositional variability and the presence of Mg-Fe cation ordering. The changes in the thermodynamic behavior may be triggered by both compositional changes and by coupling with the non-convergent process of Mg-Fe cation order. It was also suggested recently that microtextural disorder coming from antiphase domains or exsolution textures might affect the transition (Tribaudino 2000; Tribaudino et al. 2001).

In this work, a synthetic clinopyroxene of composition $Ca_{0.15}Mg_{1.85}Si_2O_6$ was investigated by using situ high-temperature single-crystal X-ray diffraction (XRD), through the $P2_1/c$ to $C2/c$ phase transition, with the following objectives: (1) to detail the thermodynamic behavior in a sample unaffected by the non-convergent cation order process and to clarify the possible effects of microtextures on the phase transition and (2) to determine the high-temperature structural evolution in a sample with a very simple composition.

* E-mail: triba@dsmp.unito.it

EXPERIMENTAL PROCEDURES

Clinopyroxene single crystals were synthesized along the join diopside-enstatite ($CaMgSi_2O_6$-$Mg_2Si_2O_6$), using gel as a starting material. The synthesis was carried out in an electric furnace (SiC resistance, Pt-PtRh 10% thermocouple) at T = 1370 °C and atmospheric pressure for 624 h. The synthesized products were examined optically and by X-ray powder diffraction, using a G670 Huber diffractometer equipped with an image plate Guinier camera (Cu$K\alpha_1$, λ = 1.54055 Å). Cell parameters, determined by least squares from 25–30 unambiguously indexed reflections measured from the powder pattern (collected in the range 5–70° 2θ) using the Unit Cell refinement program (Holland and Redfern 1997), are: a = 9.652(1) Å, b = 8.845(1) Å, c = 5.203(1) Å, β = 108.37(2)°.

The composition of the synthetic clinopyroxene was determined using a Cambridge S360 electron microprobe, equipped with a Link Analytical QX2000 EDS unit. The standards for Mg, Si, and Ca were natural MgO, SiO_2, and $CaSiO_3$, respectively. ZAF 4 corrections were applied to the analyses.

A microprobe analysis performed on one of the two crystals used for high-temperature in situ heating (dien2, after heating) gave $Ca_{0.15(1)}Mg_{1.85(1)}Si_{2.00(1)}$. The same composition was found in another crystal that was not used for the single-crystal investigation.

Single crystals with sharp optical extinction were chosen for the high-temperature investigation and these were subsequently tested on the single-crystal diffractometer. The main problem in selecting a suitable sample was (100) twinning, revealed by the presence of split reflections. Two crystals were eventually chosen: dien1 (0.17 mm × 0.09 mm × 0.09 mm) and dien2 (0.17 mm × 0.15 mm × 0.15 mm.) Both crystals were annealed in situ using a microfurnace purposely built in the workshop of the Department of Earth Sciences at Cambridge University. Temperatures up to 1150 °C and intensity data in the 2θ range 3–58° can be collected with this furnace. Temperature calibration was carried out against materials with different melting points [$Co(NO_3)\cdot 6H_2O$, CH_3COONa, citric acid, Se, ZnI_2, KI, NaCl, oxalic acid, NaF, Na_2SO_4,KIO_3] before starting the heating experiments and repeated at the end. The temperature error of the furnace was estimated to be ~6 at 500 °C and ~14 at 1000 °C.

The crystals were put in sealed quartz vials (1 mm diameter). To avoid any mechanical stress, each crystal was kept in position within the vial using quartz wool.

The X-ray diffraction intensity data and cell parameters were collected with a Philips PW1100 automated four-circle diffractometer equipped with graphite-monochromatized Mo$K\alpha$ X-radiation and operating at 55 kV and 30 mA. Starting from room T, lattice parameters were measured by centering 24 selected hkl a reflections ($h + k$ = 2n) in the θ-range 6–20°. After this, the intensities of five b reflections ($h + k$ = 2n + 1: 102, 052, $\bar{7}02$, $\bar{2}\bar{3}3$, $\bar{2}33$) were determined using ω-rotations (with 3° step scan profile). For scaling purposes, the intensities of adjacent a reflections in the same reciprocal row (202, 062, $\bar{6}02$, $\bar{1}\bar{3}3$, $\bar{1}33$) were also measured. The cell parameters and the ratio of the sum of the five measured a and b reflections (I_b/I_a) are reported in Tables 1, 2, and 3.

Crystal dien1 was heated to the temperature limit of the

TABLE 1. Cell parameters vs. temperature in dien1 sample

T(°C)	a (Å)	b (Å)	c (Å)	β (°)	V(Å³)	I_b/I_a
25	9.665(3)	8.861(3)	5.211(2)	108.38(3)	423.5(3)	0.734
35	9.664(4)	8.860(3)	5.212(2)	108.37(2)	423.5(3)	0.735
50	9.670(4)	8.865(4)	5.212(1)	108.41(3)	423.9(3)	0.734
100	9.674(3)	8.869(4)	5.215(2)	108.42(2)	424.5(3)	0.713
200	9.684(3)	8.882(3)	5.219(1)	108.46(3)	425.8(2)	0.685
300	9.694(4)	8.893(4)	5.225(2)	108.52(2)	427.1(3)	0.653
400	9.700(3)	8.902(4)	5.231(1)	108.53(2)	428.2(3)	0.618
500	9.714(4)	8.916(4)	5.237(2)	108.59(2)	429.9(3)	0.575
600	9.728(5)	8.930(3)	5.245(2)	108.66(3)	431.7(3)	0.532
700	9.740(4)	8.939(3)	5.253(2)	108.74(3)	433.1(3)	0.493
800	9.758(5)	8.955(4)	5.263(1)	108.84(3)	435.3(3)	0.437
850	9.767(5)	8.963(2)	5.270(2)	108.92(4)	436.4(3)	0.393
900	9.772(4)	8.967(4)	5.276(3)	108.99(2)	437.1(4)	0.364
950	9.788(5)	8.973(3)	5.280(3)	109.07(3)	438.3(4)	0.310
1000	9.874(4)	8.967(4)	5.336(2)	110.00(3)	444.0(3)	0.003
1025	9.877(5)	8.968(3)	5.337(3)	110.02(4)	444.2(4)	n.m.
1050	9.880(5)	8.973(3)	5.338(3)	110.01(3)	444.7(4)	n.m.
1075	9.883(4)	8.973(3)	5.336(3)	110.03(2)	444.6(4)	n.m.
1100	9.885(6)	8.978(3)	5.339(3)	110.03(3)	445.2(4)	n.m.
1125	9.888(5)	8.980(4)	5.339(3)	110.05(4)	445.4(4)	n.m.
1150	9.887(5)	8.982(4)	5.338(4)	110.05(4)	445.3(5)	n.m.
1000	9.793(5)	8.978(4)	5.284(3)	109.15(3)	438.9(5)	0.264
1025	9.876(5)	8.964(3)	5.335(3)	110.02(3)	443.8(4)	n.m.
1015	9.872(5)	8.966(4)	5.334(3)	110.00(5)	443.6(4)	n.m.
1005	9.794(6)	8.976(4)	5.287(3)	109.18(3)	439.0(4)	0.252
1038*	9.786(8)	8.976(4)	5.285(4)	109.10(4)	438.7(3)	0.339
1038†	9.876(7)	8.965(3)	5.334(3)	110.02(4)	443.7(3)	n.m

Note: I_b/I_a is the ratio of a and b reflections. The abbreviation n.m. indicates intensities not measured.
* $P2_1/c$.
† $C2/c$.

TABLE 2. Cell parameters vs. temperature in the dien2 sample during first heating

T(°C)	a (Å)	b (Å)	c (Å)	β (°)	V(Å³)	I_b/I_a
25	9.663(9)	8.856(4)	5.203(3)	108.39(5)	422.5(5)	0.742
50	9.662(10)	8.861(4)	5.206(3)	108.38(4)	423.0(5)	0.739
100	9.667(9)	8.867(3)	5.208(3)	108.41(4)	423.6(5)	0.716
300	9.689(9)	8.888(5)	5.218(2)	108.51(4)	426.1(5)	0.655
500	9.710(8)	8.911(5)	5.231(2)	108.59(3)	429.0(5)	0.580
550	9.717(7)	8.921(6)	5.237(3)	108.63(4)	430.2(5)	0.553
600	9.724(7)	8.928(6)	5.240(2)	108.66(4)	431.0(5)	0.537
650	9.725(7)	8.930(5)	5.243(2)	108.68(4)	431.3(4)	0.518
700	9.739(5)	8.938(7)	5.250(4)	108.76(4)	432.7(5)	0.497
800	9.750(6)	8.951(6)	5.256(2)	108.84(4)	434.1(4)	0.442

Note: At 850, 900, and 950 °C the cell parameters were not refined but the intensities were measured (respectively I_b/I_a = 0.434, 0.398, 0.382).

TABLE 3. Cell parameters vs temperature in the dien2 sample during reheating (see text)

T(°C)	a (Å)	b (Å)	c (Å)	β (°)	V(Å³)	I_b/I_a
250	9.675(8)	8.879(6)	5.212(3)	108.40(4)	424.8(5)	0.684
450	9.699(7)	8.903(4)	5.227(3)	108.51(4)	428.0(4)	0.622
750	9.728(7)	8.936(7)	5.239(3)	108.64(4)	431.5(5)	n.m.
975	9.757(5)	8.960(6)	5.260(3)	108.84(4)	435.2(4)	0.416
1000	9.764(6)	8.964(7)	5.264(3)	108.90(4)	435.9(5)	0.401
1050	9.765(5)	8.963(8)	5.266(3)	108.90(4)	436.1(5)	0.397
1100	9.773(6)	8.970(7)	5.271(3)	109.00(5)	436.9(5)	0.364
1125	9.783(6)	8.972(7)	5.277(3)	109.08(5)	437.7(5)	0.333
1150	9.790(5)	8.977(9)	5.283(4)	109.13(5)	438.7(4)	0.300
1100	9.778(6)	8.970(9)	5.275(4)	109.03(5)	437.4(4)	n.m.
1100	9.777(4)	8.971(7)	5.274(3)	109.04(4)	437.3(5)	0.340
1050	9.769(5)	8.965(7)	5.268(3)	108.97(4)	436.3(5)	0.384
1000	9.764(4)	8.961(7)	5.266(3)	108.90(4)	435.9(5)	0.416
950	9.754(5)	8.955(6)	5.259(3)	108.86(5)	434.7(4)	0.439
900	9.746(7)	8.952(7)	5.253(4)	108.77(5)	433.9(6)	0.462
800	9.734(6)	8.940(7)	5.248(3)	108.71(4)	432.6(5)	0.513
700	9.720(7)	8.923(5)	5.240(3)	108.64(4)	430.6(5)	0.552
600	9.712(7)	8.917(7)	5.234(3)	108.59(5)	429.6(5)	0.582
500	9.701(6)	8.907(5)	5.228(3)	108.53(4)	428.3(4)	0.614
700	9.723(5)	8.930(7)	5.242(3)	108.64(4)	431.3(5)	n.m.

Note: The abbreviation n.m. indicates intensities not measured. At 1125 and 1150 °C during cooling, only the intensities were measured and I_b/I_a were respectively 0.309 and 0.575.

microfurnace; lattice parameters were refined and the intensities of the *a* and *b* reflections were collected at the temperature steps reported in Table 1. Subsequent cooling was then performed in order to try to determine the transition temperature accurately. Complete collection of intensity data for crystal dien1 was performed at 1038 °C and then at room temperature after the sample cooled.

After a complete data collection at room temperature, crystal dien2 was heated to 500 °C, and a complete data collection was performed at 500 °C. The procedure was repeated at 800 °C and at 1000 °C. During data collection at 1000 °C there was a power failure in the furnace and the crystal cooled down. As for crystal dien1, cell parameters and intensities of the *a* and *b* reflections were determined at the steps given in Table 2. Crystal dien2 was then heated up to the temperature limit of the furnace (Table 3). At the end, the crystal was cooled to 650 °C, with subsequent collection of intensity data.

All the heating and cooling experiments were done within the two-pyroxene field of the join diopside-enstatite (Gasparik 1990).

Unit-cell dimensions before each data collection were determined using a locally improved version (Cannillo et al. 1983) of the Philips LAT routine by centering no less than 50 reflections in the range $-28° < \theta < 28°$. The lattice parameters obtained are reported in Table 4 and are smaller than those reported for the same crystals at equivalent temperatures in Tables 1, 2, and 3. The non-correspondence in lattice parameters in Tables 1 through 4 at the same temperature is because of the different centering procedures between Tables 1–3 vs. Table 4. The procedure of Table 4 is much slower, but more suitable for single-crystal centering, using mainly high θ data with well-separated Mo$K\alpha_1$ contributions. The other procedure is faster (for Tables 1, 2, 3) and uses mainly strong reflections at low or intermediate theta, centered on average Mo$K\alpha$. As a result, the former procedure gives a smaller cell size; the internal consistency in Tables 1, 2, and 3 is preserved by always using the same set of data. Two equivalent monoclinic reflections (*hkl* and $h\bar{k}l$) were collected at a scanning speed of 5.4°/min in ω-scan mode in the θ range 2–35° at room temperature, and in the θ range 2–

TABLE 4. Cell parameters and information on the structure refinement of the crystals studied

Crystal	dien1		dien2				
T(°C)	1038	25	25	500	650	800	1000
a (Å)	9.773(5)	9.651(2)	9.651(2)	9.702(4)	9.713(4)	9.739(4)	9.752(4)
b (Å)	8.962(4)	8.846(2)	8.846(2)	8.903(3)	8.913(5)	8.936(4)	8.949(5)
c (Å)	5.271(3)	5.202(2)	5.202(1)	5.228(3)	5.234(2)	5.249(3)	5.255(3)
β (°)	108.99(5)	108.34(2)	108.38(2)	108.58(3)	108.64(3)	108.80(3)	108.84(4)
θ-range (°)	2–27	2–35	2–35	2–28	2–28	2–28	2–28
no. of total refl.	2083	4065	4036	2253	2262	2277	2281
no. of unique refl.	937	1866	1858	1018	1022	1030	1032
Rsym	11.14	2.25	2.73	4.21	6.88	5.59	6.20
R% (4σ)	8.83	2.80	3.54	3.12	5.16	4.09	4.81
R% (all)	18.11	4.76	6.17	6.17	10.47	8.83	10.48
w*R*2	15.83	5.72	7.45	6.51	10.56	7.11	8.93
GooF	1.080	0.952	1.114	1.016	1.045	0.992	1.064

TABLE 5. Selected bond distances (Å) and angles (°)

Crystal	dien1		dien2				
T(°)	1038	25	25	500	650	800	1000
TA-O2A	1.591 (8)	1.588 (1)	1.588 (2)	1.591 (2)	1.591 (4)	1.586 (3)	1.592 (3)
TA-O1A	1.614 (8)	1.611 (1)	1.611 (2)	1.607 (3)	1.606 (4)	1.611 (3)	1.611 (4)
TA-O3A	1.623 (7)	1.647 (1)	1.648 (2)	1.646 (2)	1.649 (4)	1.646 (3)	1.642 (3)
TA-O3A	1.675 (7)	1.664 (1)	1.664 (2)	1.661 (3)	1.653 (4)	1.655 (3)	1.656 (4)
	1.626	1.628	1.628	1.626	1.625	1.624	1.626
Basal tilt TA	4.70 (9)	3.81 (2)	3.73 (2)	4.13 (4)	4.22 (5)	4.40 (5)	4.52 (5)
TB-O2B	1.583 (8)	1.589 (1)	1.590 (2)	1.586 (2)	1.586 (4)	1.584 (3)	1.583 (4)
TB-O1B	1.610 (8)	1.617 (1)	1.616 (2)	1.621 (3)	1.624 (4)	1.615 (3)	1.616 (4)
TB-O3B	1.661 (8)	1.670 (1)	1.672 (2)	1.665 (2)	1.667 (4)	1.666 (3)	1.663 (3)
TB-O3B	1.687 (7)	1.675 (1)	1.673 (2)	1.671 (2)	1.671 (4)	1.667 (3)	1.665 (4)
	1.635	1.638	1.638	1.636	1.637	1.633	1.632
Basal tilt TA	5.99 (8)	6.30 (2)	6.39 (2)	6.46 (4)	6.39 (5)	6.53 (4)	6.24 (5)
M1-O2A	2.035 (9)	2.017 (1)	2.017 (2)	2.027 (3)	2.031 (4)	2.038 (3)	2.037 (4)
M1-O1A	2.067 (9)	2.041 (1)	2.039 (2)	2.051 (3)	2.053 (4)	2.054 (3)	2.062 (4)
M1-O2B	2.068 (8)	2.047 (1)	2.047 (2)	2.060 (3)	2.061 (4)	2.067 (3)	2.066 (4)
M1-O1B	2.071 (7)	2.067 (1)	2.068 (2)	2.066 (3)	2.067 (4)	2.070 (3)	2.071 (4)
M1-O1A	2.182 (8)	2.146 (1)	2.147 (2)	2.171 (2)	2.174 (4)	2.190 (3)	2.190 (4)
M1-O1B	2.253 (8)	2.177 (1)	2.177 (2)	2.204 (2)	2.210 (4)	2.222 (3)	2.231 (4)
	2.113	2.082	2.083	2.097	2.099	2.107	2.109
M2-O2B	2.030 (9)	2.010 (1)	2.005 (2)	2.018 (3)	2.024 (4)	2.024 (3)	2.034 (4)
M2-O1B	2.118 (8)	2.095 (1)	2.094 (2)	2.106 (2)	2.104 (4)	2.110 (3)	2.111 (4)
M2-O2A	2.094 (8)	2.080 (1)	2.081 (2)	2.082 (3)	2.081 (4)	2.082 (3)	2.076 (4)
M2-O1A	2.155 (8)	2.128 (1)	2.127 (2)	2.146 (3)	2.149 (4)	2.151 (3)	2.163 (4)
M2-O3A	2.422 (8)	2.302 (1)	2.301 (2)	2.346 (3)	2.356 (4)	2.387 (3)	2.393 (4)
M2-O3B	2.727 (8)	2.490 (1)	2.492 (2)	2.577 (3)	2.594 (4)	2.654 (3)	2.684 (4)
M2-O3B	2.944 (9)	3.049 (1)	3.049 (2)	3.014 (3)	3.006 (5)	2.983 (3)	2.958 (5)
	2.410	2.357	2.357	2.378	2.382	2.395	2.398
O3A-O3A-O3A	190.7 (6)	199.1 (1)	199.2 (1)	196.3 (2)	195.7 (3)	193.7 (3)	193.0 (3)
O3B-O3B-O3B	151.8 (6)	143.0 (1)	143.1 (1)	146.3 (3)	146.9 (3)	149.0 (2)	150.5 (3)

28° at high temperature. Intensity profiles were integrated following the method of Lehmann and Larsen (1974), modified by Blessing et al. (1974). The intensities were corrected for Lorentz and polarization factors, and for absorption following North et al. (1968). Weighted full-matrix least-squared refinements were done using SHELX-97 (Sheldrick 1997). For sites not involved in chemical substitutions, scattering curves for neutral atoms were used and their partial occupancies were refined with the restraint of full occupancy for the sites, following the recommendations of Hawthorne et al. (1995); sites involving substitution used fully ionized atom species. Scattering factors were taken from the *International Tables for X-ray Crystallography* (Wilson 1995). Fully ionized scattering factors were taken from Tokonami (1965). High-temperature lattice parameters and information from the structure refinements are reported in Table 4 and selected bond distances and angles are reported in Table 5. Site occupancies for the M2 site were refined without significant change with temperature (Table 6[1]). Positional and displacement parameters, reported in Table 6, and observed and calculated structure factors have been deposited.

The synthetic sample was prepared for TEM observations by crushing in an agate mortar and subsequent deposition in a holey carbon film. The TEM observations were made with a CM12 electron microscope operating at 120 kV and equipped with energy-dispersive spectrometer (EDS) analytical system and double tilt holder. For each grain examined SAED (selected-area electron diffraction) patterns were imaged and EDS analysis was conducted with an intermediate spot size (1000 Å) on the same area where the SAED patterns were taken.

RESULTS

High-temperature single-crystal investigation

The two crystals showed different behavior at the $P2_1/c$-$C2/c$ phase transition. In crystal dien1, annealed without intermediate data collection over approximately two hours, cell parameters changed significantly between 950 and 1000 °C (Fig. 1), with a strong increase in a and c parameters, a smaller but significant decrease in the b parameter, and a significant increase in the β angle (about 1°). Analysis of the values of I_b/I_a with increasing temperature (Fig. 2a) showed a continuous decrease up to 950 °C and a sudden drop at 1000 °C, indicating that a phase transition from $P2_1/c$ to $C2/c$ structure had taken place. After further heating up to 1150 °C, the crystal was cooled to 1000 °C, the temperature at which the $C2/c$ structure was observed during the previous heating, but this time the space group was determined to be $P2_1/c$. The transition was then observed between 1005 and 1015 °C during reheating. During a subsequent data collection performed at 1038 °C to obtain the HT-$C2/c$ structure, the symmetry changed again from $C2/c$ to $P2_1/c$. As shown in Figure 2a the intensities of the b reflections at 1038 °C are significantly higher than expected from mere extrapolation of those found at lower temperatures. Further heating up to the limit of the furnace did not induce the transition and a full data collection was performed at 1038 °C in $P2_1/c$, followed by a further data collection at room temperature.

For the other crystal, dien2, the heating process took much longer, as full structural data collections were performed at 500, 800, and 1000 °C during heating (about two days for each data collection). The intensities of the b reflections are the same as for the first crystal up to about 800 °C, but are slightly higher between 800 and 1000 °C, as can be seen in Figure 2b. An initial data collection at 1000 °C was interrupted owing to power failure. During reheating the intensities of the hkl with $h + k$ odd reflections were higher than during the first heating (Fig. 2b) and the phase transition, which could not be achieved due to the upper temperature limit of the furnace, was estimated to be at about 1200 °C. Therefore, T_{tr} of dien2 appeared to be higher than that of crystal dien1. During subsequent cooling no further change in the intensities of b reflections was observed.

As shown in Figure 2, two different trends thus have to be considered. The first trend, shown as full triangles in Figure 2a, is that corresponding to the initial heating of the dien1 crystal up to 1000 °C. This trend matches that followed by crystal dien2 up to 800 °C and points to a discontinuous phase transition at a temperature between 950 and 1000 °C. This temperature is in agreement with previous determinations by Perrota and Stephenson (1965) and by Schwab and Schwerin (1975) on crystals synthesized at high T with the same composition as the sample in this study.

The transition behavior can be modeled using the evolution of the macroscopic order parameter Q, which can be retrieved from the intensity of the b reflections as $I \propto Q^2$ (Salje 1992). The evolution of the order parameter Q below the transition temperature (T_{tr}) can be described by the standard Landau expansion as follows:

$$G = \frac{1}{2}a(T - T_c)Q^2 + \frac{1}{4}bQ^4 + \frac{1}{6}cQ^6 \quad (1)$$

At equilibrium

$$\frac{\Delta G}{\partial Q} = 0 = a(T - T_c)Q + bQ^3 + cQ^5 \quad (2)$$

$$T = T_c - \frac{b}{a}Q^2 - \frac{c}{a}Q^4. \quad (3)$$

Considering $I \propto Q^2$ and intensity ratio data up to 950 °C as a simple polynomial fitting to intensity data yielded $T = 926(39) + 1026(154)Q^2 - 3063(148)Q^4$. The critical temperature (T_c) obtained is lower than the observed T_{tr}, which should be between 950 and 1000 °C, as it occurs for a first order transition. Also, as ratio b/a is positive, b is negative. At T_{tr} there is a jump in Q from zero to Q_0. Thus, the equilibrium variation of Q can be described by:

$$Q^2 = \frac{2}{3}Q_0^2\left\{1 + \left[1 - \frac{3}{4}\left(\frac{T - T_c}{T_{tr} - T_c}\right)\right]^{1/2}\right\}. \quad (4)$$

Values of $Q_0^2 = 0.2526$ and $T_{tr} = 991$ °C can be obtained

[1]For a copy of Table 6, document item AM-02-006, contact the Business Office of the Mineralogical Society of America (see inside front cover of recent issue) for price information. Deposit items may also be available on the American Mineralogist web site at http://www.minsocam.org.

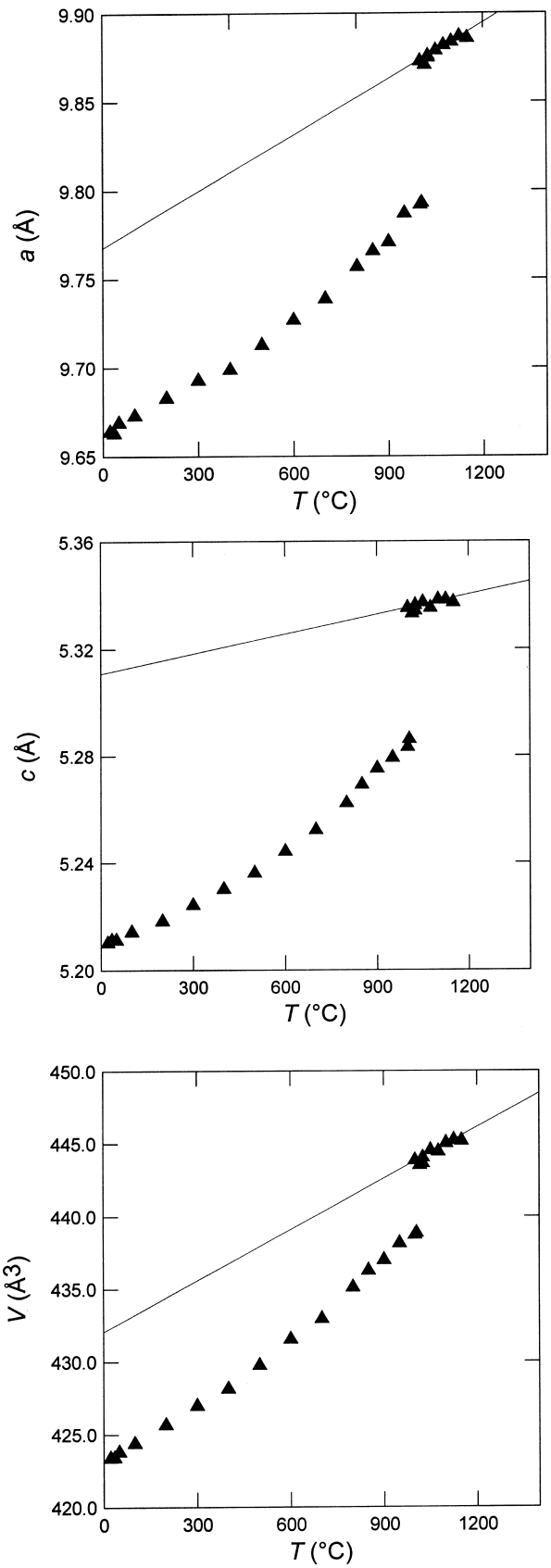

FIGURE 1. Cell parameters vs. *T* for the crystal dien1, first heating (full triangles in all figures). The extrapolation from *C*2/*c* H*T* data is shown as solid line.

from the following expressions:

$$Q_0^2 = \frac{4a}{b}(T_{tr} - T_c) \tag{5}$$

$$(T_{tr} - T_c) = \frac{3b^2}{16ac}. \tag{6}$$

The second trend to be considered is that of crystal dien2 (open diamonds in Fig. 2b) during the reheating after the data collection failure at 1000 °C. The transition temperature is higher and although in this case data for the transition could not be obtained, first-order behavior is revealed by fitting the measured data as follows: T = 1077(72) + 1392(306)Q^2 – 3808(313)Q^4. The transition temperature can be calculated with the expression used above, which yields T_{tr} = 1172 °C, i.e., a temperature beyond our highest temperature datum of 1150 °C. We also obtained a slightly higher value of 0.2758 for Q_0^2 com-

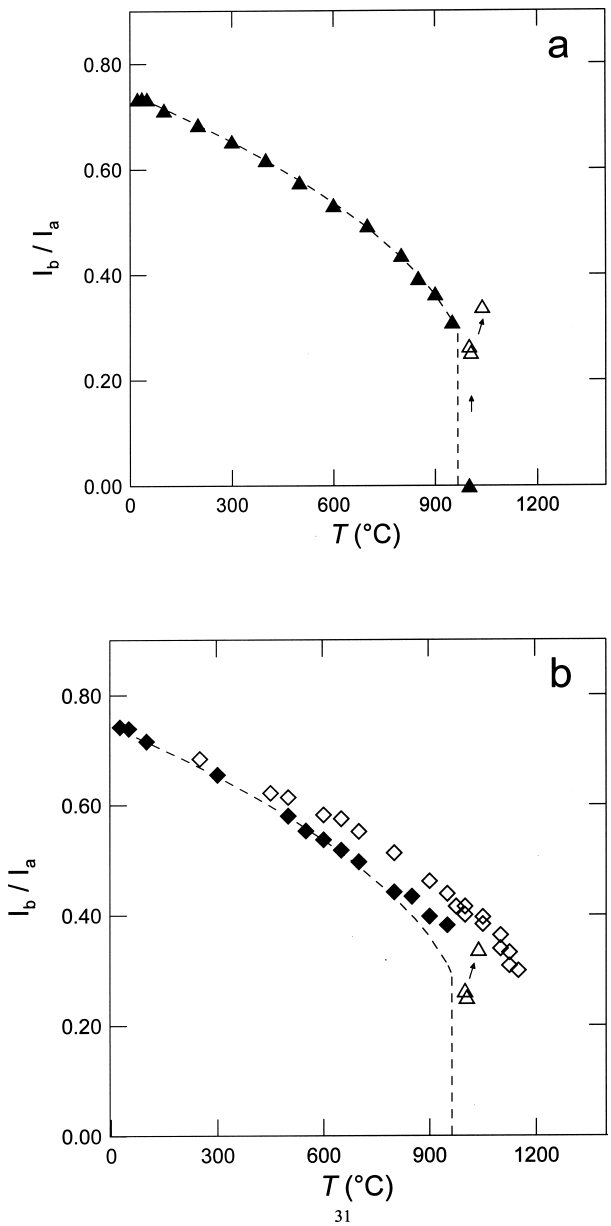

31

FIGURE 2. Evolution with T of the ratio of the intensity of hkl with $h + k$ odd and with $h + k$ even reflections (I_b/I_a) for both crystals (**a**) dien1; (**b**) dien2. In (**a**) $P2_1/c$ data for crystal dien1 before the transition are given as full triangles, those after the transition are given as open triangles reported also in (**b**), with arrows indicating the evolution with heating. In (**b**) $P2_1/c$ data for crystal dien2 referring to the first heating and data collection are given as full diamonds, those referring to heating after power failure during collection at 1000 °C are given as open diamonds. Note that the first heating data follow the same trend in dien1 as in dien2 up to $T \approx 800$ °C. In both figures the broken line corresponds to the Landau first order trend for dien1, first heating. The precision in the temperature measurement of the furnace is smaller than the dimension of the symbols.

pared to that of 0.2526 for dien1. Both (T_{tr}-T_c) and Q_0^2 for crystal dien2 indicated that after prolonged heating at 1000 °C the transition was still far from being tricritical.

This transition temperature is in better agreement with the data of Prewitt et al. (1971) who noted that the T_{tr} = 990 °C value obtained by Perrota and Stephenson (1965) was lower than the transition temperature that could have been retrieved by extrapolation of the transition temperature that Prewitt et al. (1971) measured on natural samples (about 1200 °C).

The behavior of the intensities measured on sample dien1 after prolonged heating at $T > 1000$ °C (open triangles in Fig. 2a) is intermediate between the two trends shown by sample dien2 in Figure 2b. In this case heating at $T > 1000$ °C switches the transition from higher to lower symmetry, and increases the intensities of the critical reflections up to the values observed in the trend outlined by crystal dien2 during reheating (open diamonds in Fig. 2b).

The analysis of the spontaneous strain tensor gave further information. The spontaneous strain associated with the transition can be calculated at a given temperature by comparison of the actual values of the $P2_1/c$ cell parameters with those extrapolated from the high-temperature $C2/c$ phase. Calculation of the spontaneous strain was limited here to sample dien1, for which high-temperature $C2/c$ cell parameters were measured in a temperature range of about 150 °C. The observed trends for cell parameters were linearly extrapolated to obtain $C2/c$ cell parameters below the transition (Fig. 1). Calculation of the spontaneous strain was performed with the **c** axis coincident with **z** of the underlying Cartesian coordinate system, the **b** axis coincident with **y** and the **a*** direction coincident with **x**. The symmetry-allowed spontaneous strain components for this transition are therefore:

$$\mathbf{e}_1 = a\sin\beta / a_0\sin\beta_0 - 1 \quad (7)$$
$$\mathbf{e}_2 = b/b_0 - 1 \quad (8)$$
$$\mathbf{e}_3 = c/c_0 - 1 \quad (9)$$
$$\mathbf{e}_4 = 0 \quad (10)$$
$$\mathbf{e}_5 = a\cos\beta / a_0\sin\beta_0 - c\cos\beta_0 / c_0\sin\beta_0 \quad (11)$$
$$\mathbf{e}_6 = 0. \quad (12)$$

Note that the equations reported above are different from those provided by Carpenter et al. (1998) due to the different setting.

The volume strain (V_s, Carpenter et al. 1998) calculated for dien1 has a linear relation with the intensity of the critical reflections (Fig. 3). In this co-elastic transition only non-symmetry breaking strain components are allowed and, in the absence of higher order coupling a $V_s \propto Q^2 \propto I_b/I_a$ relation was expected, in accordance with Carpenter et al. (1998). Optimum fitting could not be obtained with our data, probably due to the limited temperature range over which the $C2/c$ cell parameters were measured. All the components of the spontaneous strain tensor showed a discontinuity at the transition (Fig. 4), in agreement with the first order character of the transition.

The spontaneous strain ellipsoid at the transition calculated for our crystals showed that the highest deformation occurred on the (010) plane, with strong expansion in a direction of about 155° from **c**. This direction corresponds to a direction of major deformation in pyroxenes (Finger and Ohashi 1976; Tribaudino

et al. 2000), which can be observed by increasing temperature and pressure. Along the other two directions of the spontaneous strain ellipsoid, i.e., along **b** and on the (010) plane, only minor compression occurred (Table 7).

Comparison with the spontaneous strain related to the analogous high-pressure transition is worth noting: data for clinopyroxenes of two different compositions along the diopside-enstatite join (Fig. 5) show that the orientation of the strain ellipsoid is very close (Angel and Hugh-Jones 1994; Tribaudino et al. 2001). The greatest deformation (here compression) occurs along the same direction, with smaller expansion along the other two axes. For both transformations the main effect is an arrangement in the M2 polyhedral configuration that induces significant chain shifting, hence significant changes in the β angle, which are the basis of the observed transformations (Hugh-Jones et al. 1994). However, the high-pressure transition occurs with much greater expansion along **b** than is the case for the corresponding compression with temperature. This behavior could be explained as an effect of the chain arrangement at high temperature and pressure (Brown et al. 1972; Hugh-Jones at al. 1994). At high temperature both chains become almost fully extended to cope with the increase in size of the M1 polyhedron. This induces a slight compression of the tetrahedral chain along **b**, best seen in a projection on the *a***-b* plane. Finally, our HT structure refinement results suggest that change of the basal tilt angle at the transition could contribute to compression along **b**.

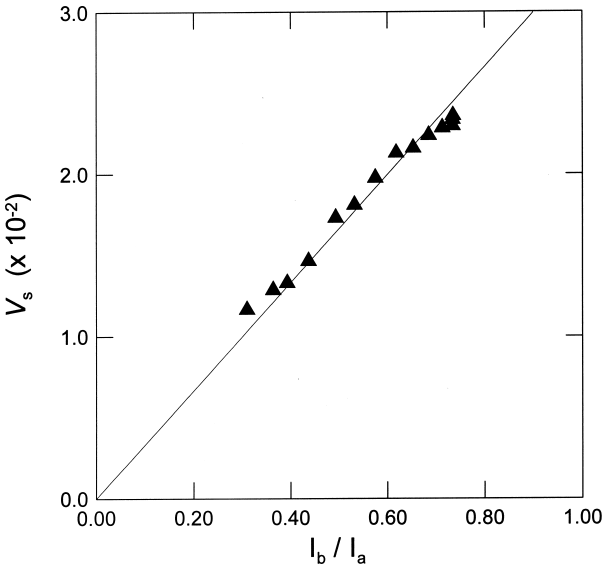

FIGURE 3. Volume strain vs the ratio of the intensity of *hkl* $h + k$ odd and $h + k$ even reflections (I_b/I_a) for crystal dien1.

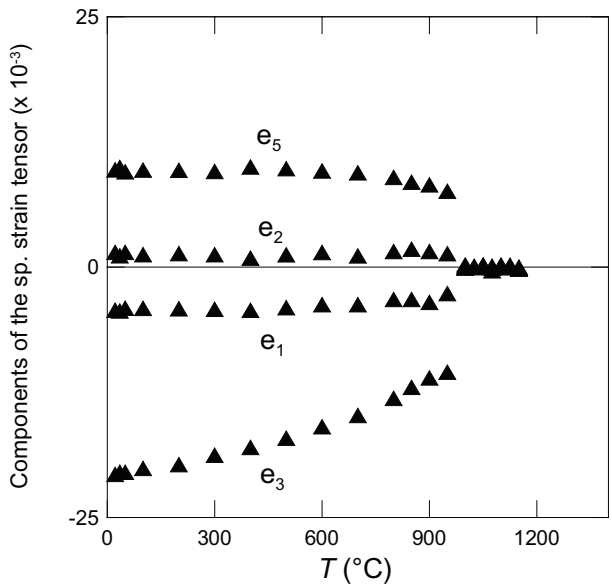

FIGURE 4. Components of the spontaneous strain tensor of the crystal dien1 vs. *T*.

Transmission electron microscopy

TEM analysis of various grains of the untreated pigeonite sample showed the presence of antiphase domains even larger than the average grain size of the crushed samples (more than 1 μ). Ribbons of antiphase domains crossing the sample were seldom observed, confirming that heating at high temperature occurred in the *C*2/*c* space group, and that a transition to $P2_1/c$ occurred during cooling. Microtwinning along (100) was observed sporadically. Selected area diffraction patterns show very sharp reflections and no exsolution texture, even in the form of a non-periodic modulation, was revealed by bright or dark field imaging.

Mottled textures were observed in volcanic pigeonite by Pasqual et al. (2000) and in Ca-rich synthetic samples along the diopside-enstatite join by Tribaudino (2000) and were interpreted as preliminary to exsolution in samples with very fast cooling. The observed combination of a lack of exsolution texture, large antiphase domains, and microtwinning is similar to that observed in pigeonite from ureilites (Tribaudino et al. 1997; Pasqual et al. 2000). In these achondritic meteorites there is clear evidence (Goodrich 1992) of a cooling history similar to

TABLE 7. Principal axes ($\times 10^{-3}$) of the strain ellipsoid, orientation of the ε_3 major axis with **c** and scalar spontaneous strain ε_{ss} ($\times 10^{-2}$) in the dien1 sample

T(°C)	ε_1	ε_2	ε_3	angle with **c** (°)	ε_{ss}
22	–1.7	–1.5	23.6	155(1)	2.4(1)
35	–1.7	–1.1	23.6	155(1)	2.4(1)
50	–1.6	–1.5	23.3	155(1)	2.3(1)
100	–1.8	–1.2	23.2	155(1)	2.3(1)
200	–1.7	–1.4	23.0	154(1)	2.3(1)
300	–1.6	–1.2	22.4	154(1)	2.2(1)
400	–1.8	–0.9	22.2	152(1)	2.2(1)
500	–2.0	–1.2	21.5	152(1)	2.2(1)
600	–2.2	–1.4	20.5	151(1)	2.1(1)
700	–2.1	–1.1	19.5	150(1)	2.0(1)
800	–2.5	–1.6	17.9	150(1)	1.8(1)
850	–2.3	–1.8	16.8	149(1)	1.7(1)
900	–2.1	–1.6	16.0	148(1)	1.6(1)
950	–2.2	–1.6	14.8	149(1)	1.5(1)
1000	–1.6	–1.4	14.1	148(1)	1.4(1)
1005	–1.5	–1.2	13.6	147(1)	1.4(1)
1038	–2.2	–0.8	14.8	147(1)	1.5(1)

Note: ε_1, ε_2, and ε_3 are the diagonalized components of the spontaneous strain tensor. ε_2 is oriented along **b**, ε_1 and ε_3 on the (010) plane, normal to each other. The orientation of the ε_3 axis on (010) is measured with the **c** axis, from **c** toward +**a** (Finger and Ohashi 1976).

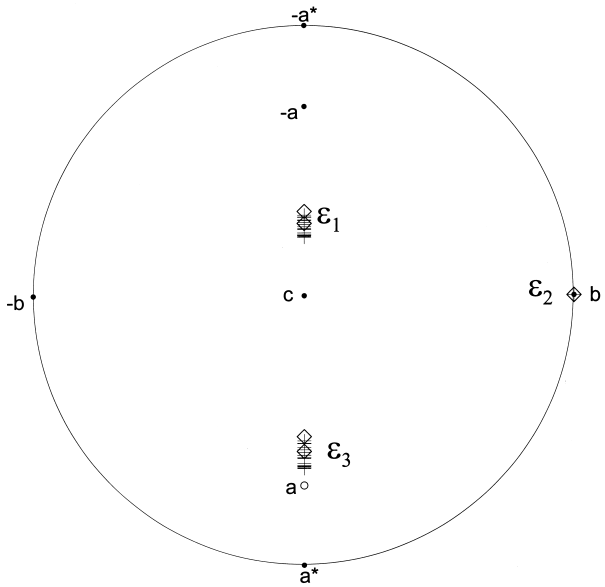

FIGURE 5. Stereographic projection of the orientation of the axes of the spontaneous strain ellipsoids. Crosses refer to the dien1 sample, diamonds to high-pressure data for the phase transition in clinoenstatite and $Ca_{0.5}Mg_{1.5}Si_2O_6$ (Angel and Hugh-Jones 1994; Tribaudino et al. 2001). The orientation of the crystallographic and strain axes is on the upper hemisphere, apart from the **a** axis (open circle).

that of our synthetic samples, i.e., prolonged heating at high temperature within the pigeonite stability field, followed by very fast cooling, possibly due to sudden breaking of the parent body, at a rate faster than what would be experienced by natural crystals in Earth conditions. Extremely fast cooling is responsible for the lack of mottled textures and very large antiphase domains (Carpenter 1979). In our samples, the presence of microtwinning and the absence of shock traces suggests that, for pigeonite, microtwinning is not in itself evidence of shock, as was suggested for Ca-rich clinopyroxenes by Hornemann and Müller (1971).

A few grains of pigeonite were annealed for 72 h at T = 1050 °C and P = 1 atm to simulate the conditions of peak heating during the single-crystal experiment. TEM observations of these treated samples showed the presence of irregular modulations, revealed by peak streaking (Fig. 6) and by dark and bright field imaging. Although the modulations are not periodic, as shown by the lack of satellite splitting in the SAD patterns (Fig. 6b), an average periodicity of 150 Å was observed. The orientation of the modulations is parallel to (101), corresponding to that of the platelets observed parallel to (101) in synthetic clinopyroxene of composition $Wo_{6-9}En_{75-79}Fs_{15-16}$, i.e., with a Ca/(Ca + Mg + Fe) value similar to our sample, cooled at a constant rate of 8/h from 1350 °C to room temperature (Feuer et al. 1989). These platelets were interpreted as related to nucleation of exsolved phases. An interpretation as incipient exsolution is also likely for our sample. However, in the study of Feuer et al. (1989), discrete platelets were present as well as a periodic modulation with satellite splitting along the main peaks, indicating periodic modulation. Distinct platelets are not present in our sample, and a higher strain is retained.

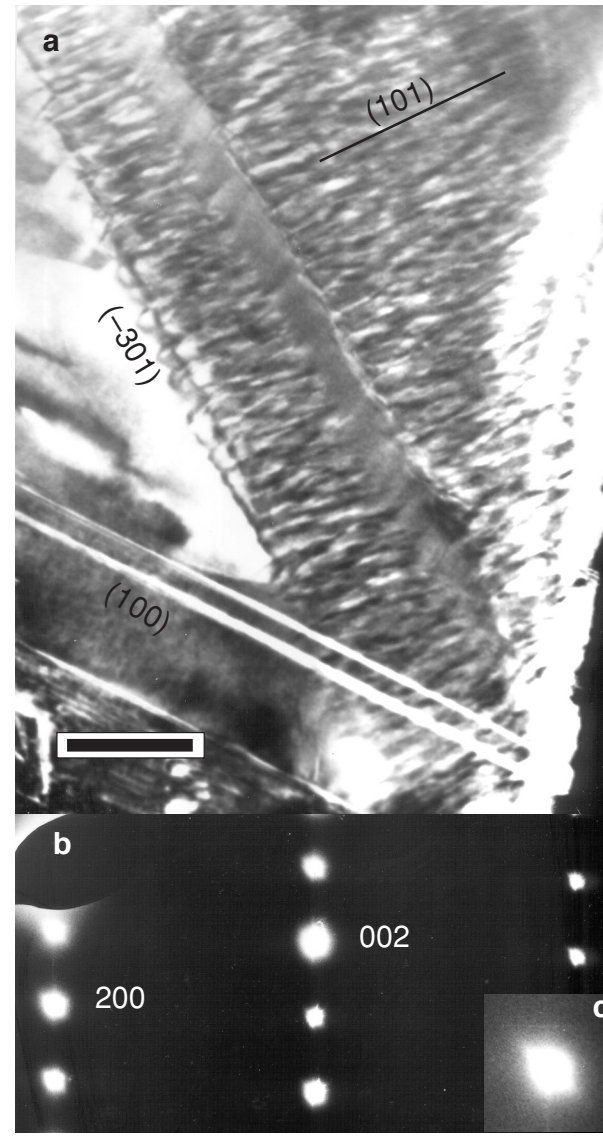

FIGURE 6. TEM examination of the $Ca_{0.15}Mg_{1.85}Si_2O_6$ clinopyroxene sample after 72 h at T = 1050 °C. (**a**) Mottled texture oriented parallel to (101); twinning along (100) and contact with modulation free areas along ($\bar{3}01$) are also shown; scale bar 1000 Å. Dark field: g = [$\bar{2}02$]. (**b**) SAD pattern on the same area as (**a**), oriented along [010]. (**c**) Detail of a diffraction spot from (**b**). Note streaking along [101]*.

The observed microtexture thus seems to be preliminary to the formation of platelets.

Modulation is not ubiquitous; as shown in Figure 6a minor areas without microtextures seem to coexist with mottled areas, with an interface between mottled and non-mottled areas oriented approximately along ($30\bar{1}$). Nevertheless, no indication of different compositions for the two areas was found, as microprobe analysis performed with minimum spot size (600 Å) did not show significant differences. The ($30\bar{1}$) orientation is almost consistent with the direction for the energy minimum of the *P*/*C* interface (Shimobayashi and Kitamura 1991). In

this case, in which both areas have $P2_1/c$ symmetry, it may be a remnant indicating a high-temperature coexistence of the $C2/c$ and $P2_1/c$ phases. Cameron et al. (1973) showed that Ca more easily enters the larger and less distorted M2 polyhedron in the H*T*-$C2/c$ structure than that of the $P2_1/c$ structure, thus suggesting that exsolution could more promptly occur in the $P2_1/c$ structure. Fainter modulation also seems to be present, however, in the non-mottled areas.

Analysis of the structural parameters

The temperature limit of our furnace and the increase in the transition temperature that was observed during heating meant that we could not collect and refine $C2/c$ phase data from our samples. We report here the results of the structural refinement of crystal dien2 at five different temperatures below the transition; geometrical features are described and discussed with reference to data from the literature (Smyth 1974; Arlt and Armbruster 1997).

It is well known that pigeonite $P2_1/c$ has two symmetry-independent tetrahedral chains: an A-chain with S-rotation (the O2-O3-O3 basal face of tetrahedra with the same orientation as the triangular faces of the octahedron to which tetrahedra are linked through the apical O1 atom), and a B-chain with O-rotation (the basal face of tetrahedra oriented opposite to the triangular face of the octahedra). Approaching the transition temperature both chains extend along **c** by rotating the basal faces of tetrahedra. This can be seen by following the variation of the angles O3-O3-O3 for both chains as shown in Figure 7a. The variation of the same angles for clinohypersthene (Smyth 1974) and kanoite (Arlt and Armbruster 1997) was reported for comparison. Within the $P2_1/c$ stability field both chains extended by about 7° and the A-chain remained S-rotated. Data from Smyth (1974) and Arlt and Armbruster (1997) show that after the discontinuous transition both chains were O-rotated. Unfortunately we could not check the same behavior for our samples as the $C2/c$ phase data were missing. A very large difference in the chain arrangement even at 1000 °C was nevertheless present in our samples, confirming the first order character of the transition.

Another interesting parameter to be analyzed was the out of plane tilting of the basal face of the tetrahedra (basal tilt). In Figure 7b the variation of this parameter with *T* shows that while the B-chain nearly maintained the same basal tilt over the studied temperature range, the basal tilt of the A-chain increased with temperature. Again, we do not have data for the basal tilt angle of the tetrahedra chain in the $C2/c$ phase but if an abrupt increase in the A-chain basal tilt angle occurred, this would explain the collapse of the *b* cell parameter observed at the transition.

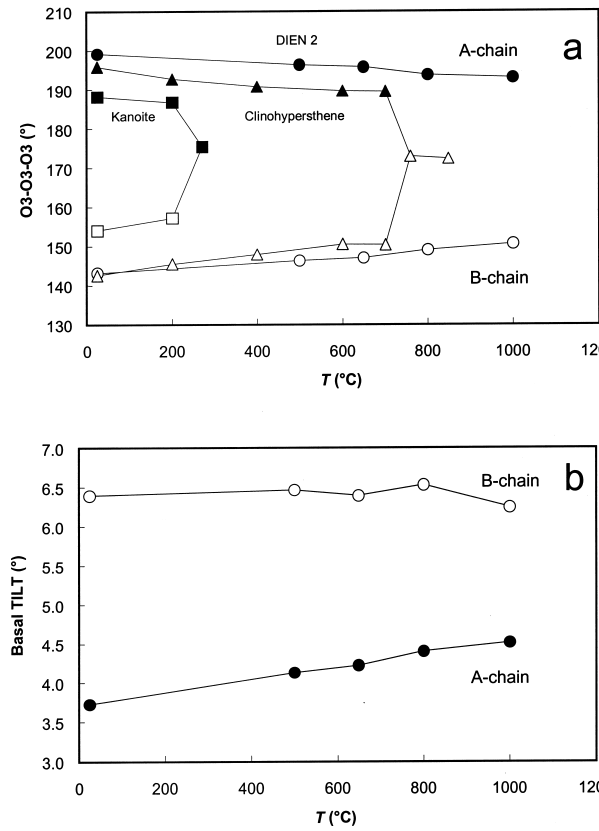

FIGURE 7. (**a**) Variation of O3-O3-O3 chain kinking angle with temperature in sample dien2, clinohypersthene (Smyth 1974), and kanoite (Arlt and Armbruster 1997). (**b**) Chain basal tilting with *T* for sample dien2.

DISCUSSION

The results of this work show the first-order character of the transition in these Fe-free pigeonites. The most intriguing result was the non-reversible increase in the T_{tr} value observed with heating at high temperature. A reversible increase in T_{tr} and a continuous behavior of the phase transition was found recently in a high-temperature investigation carried out on Fe-rich pigeonite with Ca content of 0.2 apfu by Cámara et al. (2002), which were related to coupling between displacive transition and cation ordering and to the higher Ca content. However, in our study, which deals with Fe-free samples, the observed behavior could only be reasonably ascribed to some effect related to the presence of Ca, as T_{tr} is related to Ca content (Prewitt et al. 1971). This is supported by the findings of Shimobayashi and Kitamura (1991), who showed that in Ca-free clinoenstatite the transition temperature did not change with repeated heating. Finally, the increase in T_{tr} must be related to some mechanism that begins to be effective at $T > 850$ °C, as the behavior of the two crystals is the same up to 800 °C (Figs. 2a and 2b), in spite of the different heating history, and such a mechanism should be related to some non-reversible change.

An increase in the transition temperature by order parameter fluctuations related to defects in minerals was discussed by Salje (1992). The exsolution features observed by TEM in our Ca-bearing sample, due to heating close to the temperature of the transition, were likely to have given rise to local order parameter fluctuations. These fluctuations, being associated with compositional fluctuations, were coupled with a strain related to incipient exsolution. Similar fluctuations were previously observed in more Ca-rich samples by Tribaudino (2000). TEM observations performed on our samples showed that a mottled texture developed during heating at high temperature,

likely due to Ca-clustering in a previously homogeneous sample.

This is in reasonable agreement with the data represented in the experimentally determined time-temperature-transformation (TTT) diagram of Nord and McCallister (1979) who observed the formation of decomposition structures after heating for a few days at a T of about 800–900 °C. The formation of preliminary spinodal decomposition was observed at a similar temperature (950–1050 °C) during heating of a crystal of pigeonite from ureilite with a composition close to that of this study (PCA82506, $Wo_6En_{76}Fs_{18}$) by Pasqual et al. (2000). In our study, this process appears to have started above 850 °C, the temperature at which the trend of crystal dien1, annealed from room T to 850 °C over about two hours and that of crystal dien2, annealed over several days to allow data collection, began to diverge. It has to be stressed that whereas the synthesis of our pigeonite sample was carried out within the stability field of Ca-poor pyroxene, the in situ heating experiments were carried out outside the stability field of the examined phase. The presence of defects may also explain the different transition temperatures detected on natural (Prewitt et al. 1971) and synthetic samples (Perrota and Stephenson 1965; Schwab and Schwerin 1975); natural crystals, which underwent rather slow cooling probably developed microtextural inhomogeneities that stabilized the $P2_1/c$ structure with respect to synthetic homogeneous samples.

ACKNOWLEDGMENTS

The authors thank R. Angel, D. Isaak, and an anonymous referee for helpful suggestions. Financial support from CNR and MURST project "Transformation, reactions, ordering in minerals" is gratefully acknowledged.

REFERENCES CITED

Angel, R.J. and Hugh-Jones, D.A. (1994) Equations of state and thermodynamic properties of enstatite pyroxenes. Journal of Geophysical Research, 99, 19777–19783.

Angel, R.J., Chopelas, A., and Ross, N.L. (1992) Stability of high-density clinoenstatite at upper mantle pressures. Nature, 358, 322–324.

Arlt, T. and Angel, R.J. (2000) Displacive phase transitions in C-centered clinopyroxenes: spodumene, $LiScSi_2O_6$ and $ZnSiO_3$. Physics and Chemistry of Minerals, 27, 719–731.

Arlt, T. and Armbruster, T. (1997) The temperature dependent $P2_1/c$-$C2/c$ phase transition in the clinopyroxene kanoite $MnMg[Si_2O_6]$: a single-crystal X-ray and optical study. European Journal of Mineralogy, 9, 953–964.

Arlt, T., Kunz, M., Stoltz, J., Armbruster, T., and Angel, R.J. (2000) P-T-X data on $P2_1/c$ clinopyroxenes and their displacive phase transitions. Contributions to Mineralogy and Petrology, 138, 35–45.

Blessing, R.H., Coppens, P., and Becker P. (1974) Computer analysis of step scanned X-ray data. Journal of Applied Crystallography, 7, 488–492.

Brown, G.E., Prewitt, C.T., Papike, J.J., and Sueno, S. (1972) A comparison of the structures of low and high pigeonite. Journal of Geophysical Research, 77, 5778–5789.

Cámara, F., Carpenter, M.A., Domeneghetti, M.C., and Tazzoli, V. (2002) Non-convergent ordering and displacive phase transition in pigeonites: *in situ* HT XRD study. Physics and Chemistry of Minerals, in press.

Cameron, M., Sueno, S., Prewitt, C.T., and Papike, J.J. (1973) High-temperature crystal chemistry of acmite, diopside, hedenbergite, jadeite, spodumene and ureite. American Mineralogist, 58, 594–618.

Cannillo, E., Germani, G., and Mazzi, F. (1983) New crystallographic software for Philips PW 1100 single crystal diffractometer. CNR Centro di Studio per la Cristallografia, Internal Report 2.

Carpenter, M.A. (1979) Experimental coarsening of antiphase domains in a silicate mineral. Science, 206, 681–683.

Carpenter, M.A., Salje, E.K.H., and Graeme-Barber, A. (1998) Spontaneous strain as a determinant of thermodynamic properties for phase transition in minerals. European Journal of Mineralogy, 10, 621–691.

Feuer, H., Schröpfer, L., Fuess, H., and Jefferson, D.A. (1989) High resolution transmission electron microscope study of exsolution in synthetic pigeonite. European Journal of Mineralogy, 1, 507–516.

Finger, L.W. and Ohashi, Y. (1976) The thermal expansion of diopside to 800 °C and a refinement of the crystal structure at 700 °C. American Mineralogist, 61, 303–310.

Gasparik, T. (1990) A thermodynamic model for the enstatite-diopside join. American Mineralogist, 75, 1080–1091.

Goodrich, C.A. (1992) Ureilites: a critical review. Meteoritics and Planetary Sciences, 27, 327–352.

Hawthorne, F.C., Ungaretti, L., and Oberti, R. (1995) Site populations in minerals: terminology and presentation of results of crystal-structure refinement. Canadian Mineralogist, 33, 907–911.

Holland, T.J.B. and Redfern, S.A.T. (1997) Unit cell refinement from powder diffraction data: the use of regression diagnostics. Mineralogical Magazine, 61, 65–77.

Hornemann, U. and Müller, W.F. (1971) Shock-induced deformation twins in clinopyroxene. Neues Jahrbuch für Mineralogie Monatshefte, 1971, 247–256.

Hugh-Jones, D.A., Woodland, A.B., and Angel, R.J. (1994) The structure of high pressure $C2/c$ ferrosilite and crystal chemistry of high-pressure $C2/c$ pyroxenes. American Mineralogist, 79, 1032–1041.

Lehmann, M.S. and Larsen, F.K. (1974) A method for location of the peaks in step-scan-measured Bragg reflections. Acta Crystallographica, A30, 580–584.

Nord, G.L. and McCallister, R.H. (1979) Kinetics and mechanism of decomposition in $Wo_{25}En_{31}Fs_{44}$ clinopyroxene. Geological Society of America, Abstracts with Programs, 11, 488.

North, A.C.T., Phillips, D.C., and Mathews, F.S. (1968) A semi-empirical method of absorption correction. Acta Crystallographica, A24, 351–359.

Pasqual, D., Molin, G., and Tribaudino, M. (2000) Single-crystal thermometric calibration of Fe-Mg order-disorder in pigeonites. American Mineralogist, 85, 953–962.

Perrota, A.J. and Stephenson, D.A. (1965) Clinoenstatite: high-low inversion. Science, 148, 1090–1091.

Prewitt, C.T., Brown, G.E., and Papike, J.J. (1971) Apollo 12 clinopyroxenes. High temperature X-ray diffraction studies. Geochimica et Cosmochimica Acta, 1, 59–68.

Salje, E.K.H. (1992) Phase transitions in ferroelastic and co-elastic crystals, p. 1–229. Cambridge University Press, Cambridge, U.K.

Schwab, R.G. and Schwerin, M. (1975) Polimorphie und entmishungsreaktionene der pyroxene im system Enstatit ($MgSiO_3$)—Diopsid ($CaMgSi_2O_6$). Neues Jahrbuch für Mineralogie Abhandlungen, 124, 223–245.

Sheldrick, G.M. (1997) Programs for Crystal Structure Analysis (Release 97-2). Institüt für Anorganische Chemie der Universität, Tammanstrasse 4, D-3400 Göttingen, Germany.

Shimobayashi, N. and Kitamura, M. (1991) Phase transition in Ca-poor clinopyroxenes: a high temperature transmission electron microscopic study. Physics and Chemistry of Minerals, 18, 153–160.

Smyth, J.R. (1974) The high temperature crystal chemistry of clinohypersthene. American Mineralogist, 59, 1061–1082.

Smyth, J.R. and Burnham, C.W. (1972) The crystal structures of high and low clinohypersthene. Earth and Planetary Science Letters, 14, 183–189.

Sueno, S., Kimata, M., and Prewitt, C.W. (1984) The crystal structure of high clinoferrosilite. American Mineralogist, 69, 265–269.

Tokonami, M. (1965) Atomic scattering factors for O^{2-}. Acta Crystallographica 19, 486.

Tribaudino, M. (2000) A transmission electron microscope investigation on the $C2/c$-$P2_1/c$ phase transition in clinopyroxenes along the diopside-enstatite ($CaMgSi_2O_6$-$Mg_2Si_2O_6$) join. American Mineralogist, 85, 707–715.

Tribaudino, M., Fioretti, A.M., Martignago, F., and Molin, G.M. (1997) Transmission electron microscope texture and crystal chemistry of coexisting ortho- and clinopyroxene in the Antarctic ureilite Frontier Mountain 90054: implications for thermal history. Meteoritics and Planetary Science, 32, 671–678.

Tribaudino, M., Prencipe, M., Bruno, M., and Levy, D. (2000) High pressure behaviour of Ca-rich $C2/c$ clinopyroxenes along the join diopside-enstatite ($CaMgSi_2O_6$-$Mg_2Si_2O_6$). Physics and Chemistry of Minerals, 27, 656–664.

Tribaudino, M., Prencipe, M., Nestola, F., and Hanfland, M. (2001) A $P2_1/c$-$C2/c$ high pressure phase transition in $Ca_{0.5}Mg_{1.5}Si_2O_6$ clinopyroxene. American Mineralogist, 86, 807–813.

Wilson, A.J.C., Ed. (1995) International Tables for Crystallography, Volume C, Kluwer Academic Publishers, Dordrecht, The Netherlands.

MANUSCRIPT RECEIVED JULY 3, 2001
MANUSCRIPT ACCEPTED DECEMBER 20, 2001
MANUSCRIPT HANDLED BY DONALD G. ISAAK